# The Use of a He-Ne Laser Calibrated by a Fourier Transform Spectrometer in the Investigation of Emission Spectra of a Hg Lamp

Martin A. He Friday 3rd February, 2023
Blackett Laboratory, Imperial College London, SW7 2AZ, United Kingdom

*Abstract* - **A Fourier Transform spectrometer (FTS) was assembled and aligned to observe and measure the peaks of a gaseous mercury discharge lamp, and a He-Ne laser (λ= 632.816nm) was added through the placement of a third beam-splitter, unifying the two input beams from the Hg lamp and He-Ne laser, as well as dividing an output beam equally amongst two photodetectors: each as filtered by a notch, and bandpass filter respectively. A cubic spline fit obtained from the He-Ne laser interferogram was used to calibrate the other, which was refined through Butterworth filters, and a Kaiser window. A Fast Fourier Transform then revealed five distinct spectral peaks of the Hg spectrum, coinciding with the Mercury I peaks to within 1Å.**

## I Introduction & Background

A Fourier Transform Spectrometer (FTS), as illustrated in Figure 1, is a variant of the Michelson interferometer, in which one mirror is movable to alter path difference between the split beams on one of the interferometer's two arms, before recombination for detection.[1]

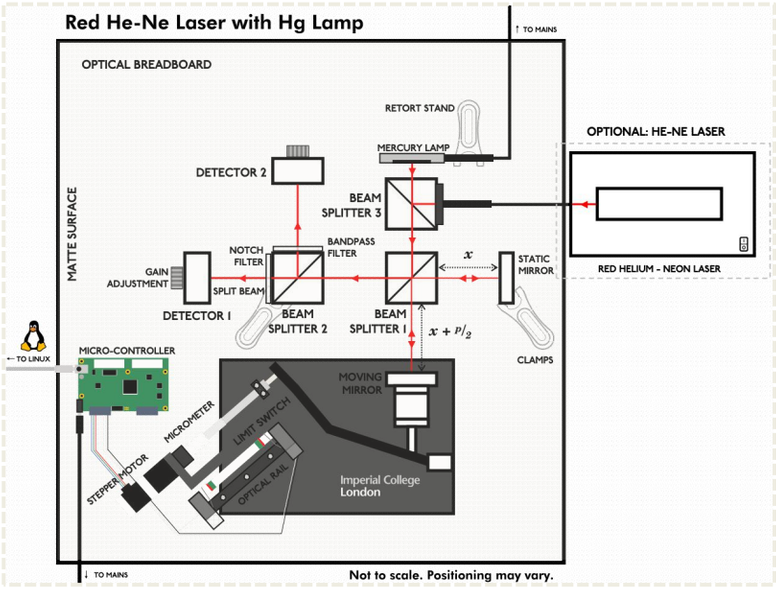


**Figure 1:** A schematic of the Fourier Transform Spectrometer (FTS) used, where the combined beam is equally divided by *Beam Splitter 2*, whilst one of the mirrors is adjustable, resulting a variable displacement of $p/2$. This introduces a path difference p to one of the split beams, before recombination by *Beam Splitter 1,* and detection by *Detectors 1* and *2*.

The FTS offers several benefits over other spectrometers[2], such as enhancing the signal-to-noise ratio *(on account of multiplex advantage gained by simultaneous measurement of all frequencies)*, the high degree of precision that can be achieved by increasing the length of the interferogram, and the ability to adjust the detector's aperture size to capture more incident light *(which improves the signal-to-noise ratio as well)*.

## II Theory

### A. Obtaining the Input Spectrum

First, we shall consider an incident beam of intensity, B(σ), where $\sigma = \lambda^{-1}$ which is called the *wavenumber* of the component of the beam. Thus, we have the obtained the resultant inteferogram, $I_R(p)$, which is given by **Equation 1**.

$$I_R(p,\sigma) = B(\sigma)[1+\cos(2\pi\sigma p)]$$

**Equation 1:** The resultant interferogram, $I_R(p)$, in terms of the wavenumber component.

Next, we shall integrate over all the incident σ, with total resultant intensity, $I_R(p)$, given by **Equation 2** in the adjacent column. This, we can then subsequently make use of in **Equation 3** to determine a certain quantity, *I(p)*, which we can take the Inverse Fourier Transform of to determine our incident beam.[3]

$$I_R(p) = \int_0^\infty B(\sigma)[1+\cos(2\pi\sigma p)]d\sigma$$

**Equation 2:** The total resultant intensity of the interferogram.

Next, we shall define a quantity, I(p), which can be found from subtracting the mean of $I_R(p)$ from our resultant interferogram in **Equation 3**.

$$I(p) \equiv I_R(p) - \overline{I_R} = \int_0^\infty B(\sigma)\cos(2\pi\sigma p)d\sigma$$

**Equation 3:** The definition of the quantity, I(p), which we observe to be the cosine FT of B(σ), the incident beam. This allows us to perform an IFT to find B(σ).

Consequently, by performing the IFT in **Equation 4**, we have B(σ).

$$B(\sigma) = \int_0^\infty I(p)\cos(2\pi\sigma p)dp$$

**Equation 4:** The inverse cosine Fourier Transform, up to a multiplicative constant, which allows us to find the incident beam, B(σ).

Now, we note the physical limitations of the system since real detectors are thus limited in terms of their sampling frequency and maximum range. Additionally, if a real detector is not exactly centered on an interferogram, this can result in a phase difference component, φ, which adds the extra term $e^{i\varphi}$ to our FT, which means to recover the input beam spectrum from a real dataset $I(p_n)$, with equally-spaced $p_n$, we can take a discrete Fourier Transform, taking its amplitude to eliminate the extra exponent phase component, in **Equation 5**.

$$B(\sigma) = \left|\sum_{n=1}^{N} I_n(p_n)e^{2\pi i\sigma p_n}\right|$$

**Equation 5:** The discrete Fourier Transform to recover from a real dataset.

This was implemented in Python, making use of the *scipy* and *numpy* libraries to perform numerical methods on our data.

## III Experimental Set-up

### A. Assembling the Fourier Transform Spectrometer

To begin with, a modified FTS was assembled as shown in **Figure 1**. This was assembled on a ThorLabs™ B6060A Nexus Breadboard. We made use of two photodetectors of OSRAM™ SFH 2200[4], custom-modified at Imperial College, which were connected to a micro-controller, and in turn interfaced with a Linux machine running a distro of Oracle™ Linux, and the package[5] *mm*, which allowed for the fine controlling of the interferometry equipment. Also connected to the micro-controller, and a Nema™ High Precision 17HS15-1684S-HG100 stepper motor[6], which was fixed to a micrometer gauge. This was placed parallel to an optical rail and limit switches which prevented the mechanism from going too far either direction. Following this, an elaborate mechanism connected to a mirror allowed for its movement, varying the path difference of one arm of the interferometer.

Two different light sources were used during this experiment: a ThorLabs™ HNL020RB He-Ne laser[7] with λ = 632.816nm, as well as UVP™ HNL020RB gaseous Hg discharge lamp[8] powered by a UVP™ Analytik Jena™ PS1 99-0055-02 18mA Power Supply. The former was placed outside of a matte-surfaced box, with a cable connecting its output with *Beam Splitter 3*, whilst the mercury lamp was placed facing the other side. This consequently combined the two light sources, which then subsequently travel to *Beam Splitter 1*. From here, the beam is equally divided between a *static mirror*, and our *moving mirror*, before recombining and heading towards *Beam Splitter 2*. At this beam-splitter, the source is divide again in two, with half passing through a *notch filter* to *Detector 1*, whilst the other half passed through a *bandpass filter* to *Detector 2*. The beam-splitters used in the experiment were the ThorLabs™ CCM1-85013/M beam-splitter[9] for λ = 400-700nm. Additionally, a ThorLabs™ LA1951-A plano-convex lens was added to one of the beam-splitters ot increase the size of the beam. Combined, this provides the set-up specified in **Figure 1**.

### B. Use of the Notch Filter

Initially, we considered the use of the notch filter, as instructed, to remove signal from the He-Ne laser, supposedly centered around approximately 600nm. However, upon further inspection, we discovered that the frequencies filtered out in actuality were below 500nm, thus removing some crucial Hg data, and we speculate that it was another bandpass filter. Therefore, for some of the runs, we proceeded with the removal of the *"notch"* filter.

### C. Adjusting the Set-Up

We adjusted the fine screws until Haidinger fringes are in focus, which indicates that our mirrors are orthogonal. Then, we observe that the stepper motor, which drives a moving mirror, moves in increments of $\mu steps$, which correspond to a movement of 15.625pm, which in turn, provided by the reduction ratios of 1:100, corresponds to a change in $p$ of 31.25pm. Our OSRAM™ SFH 2200 detectors were set to capture at a rate of 50Hz.

### D. The Nquist Theorem

Next, we must consider the Statistics of the Nyquist Theorem, whereby each oscillation of the interferogram must be measured at least twice in order to obtain clean data. By visual inspection, we have easily fulfilled this requirement, well below the Nyquist Limit.

### E. Finding the Null Point

Our null point, corresponding to $p = 0$, was located manually by visual inspection, as well as with the help of the stepper motor, in order to determine a suitable range for which to scan the interferogram, such that the null point roughly coincided with the interferogram's centre. We proceed at a speed of 60,000 $\mu steps.s^{-1}$, over various ranges, typically about 300,000,000, which corresponds to T ≅ 83 minutes. We therefore obtained a set of data, $I(\mu_n)$, from our unfiltered *(or notch-filtered)* beam component, and $R(\mu_n)$, from the $\lambda = 632.816$nm beam component, collected for the same values of $\mu_n$ where $\mu_n$ represents the number of micro-steps traversed by our stepper motor. To clean the data, we decided to discard the first and last few million micro-steps, in which the motor was accelerating.

## IV Improving the Obtained Interferogram

### A. Reducing the Effects of Noise and Misalignment

Evidently, we wish for the reduction in the amount of noise present in our set-up, an example of a limitation in the FTS, which results in differences between what was measured, and the theoretical *(real)* interferogram, which we shall denote as $I_R(p_i)$. These small misalignments could result in a shift of $p_i$ in the effective mean.

Therefore, we utilise digital Butterworth filters[10], which contain almost ideal pass-band transmission, with very little stop-band transmission. Consequently, we may make use of a high-pass filter for misalignment correct, whilst a low-pass filter can be used for the removal of high-frequency wave noise. We may wish to calculate the contribution to the interferogram by a $\lambda = 400$nm frequency:

$$f = \frac{v}{\lambda} = \frac{50,000\ \mathrm{s}^{-1} \times 31.25\mathrm{pm}}{400\ \mathrm{nm}} \cong 4\ \mathrm{Hz}$$

**Equation 6:** The contribution to the interferogram from the λ = 400nm frequency.

We wish to avoid filtering any visible sections of the spectrum, where much of the crucial Hg spectrum data lies. This was accomplished through the use of a second-order digital Butterworth filter, in which we set the cut-off frequencies to be a low-pass filter of 1Hz, and optionally a second high-pass filter with 8Hz, roughly corresponding to $\lambda = 1{,}600$nm and $\lambda = 200$nm respectively. The use of this filter also results in an output interferogram with a mean value of zero.

### B. Calibration of Path Difference between Beams

For a monochromatic input of wavelength $\lambda$, we can express it in terms of Dirac Delta function given by **Equation 7** below.[11]

$$B(\sigma) = \delta\left(\frac{1}{\lambda}\right)$$

**Equation 7:** The Dirac Delta representation of a monochromatic wavelength of light, $\lambda$.

The equation has zeros at $p = ½(x + ½)\lambda\ \forall\ x \in \mathbb{Z}$, therefore $\Delta p = ½\lambda$ for the crossing points of the *p-axis*. We can thus use a cubic-spline interpolation of the interferogram for the red He-Ne laser. We then used these values to solve for $p_n$ in the interferogram, which leads to obtaining the data $I(p_i)$, as required.

This is outlined in **Section IV.C**, as well as **Equations 8** to **10**.

### C. Reduction of Spectral Leakage

We were only able to measure a limited section of the FFT, due to its being an infinite interferogram, according to the values of $p_n$ we found from the set-up. Thus, from our discrete $p_n$ we obtain $I(p)$, the true interferogram, being multiplied by a Dirac comb. This range of $p_n$ results in the further multiplication by a rectangular window, which when FT'd is equivalent to the convolution of this real spectrum with the Fourier Transform of the Dirac comb[12] and the rectangular window, shown in its respective parts by **Equation 8, 9** and **10**.

$$s(t) = t_s \cdot \sum_{n=-\infty}^{\infty} \delta(t - t_s \cdot n) = \sum_{n=-\infty}^{\infty} \mathrm{e}^{2\pi \mathrm{j} n t / t_s}$$

$$S(f) = \mathcal{F}\left\{ t_s \cdot \sum_{n=-\infty}^{\infty} \delta(t - t_s n) \right\}(f) =$$

$$t_s \cdot \int_{-\infty}^{\infty} \sum_{n=-\infty}^{\infty} \delta(t - t_s n) \mathrm{e}^{-2\pi \mathrm{j} f t}\, \mathrm{d}t = \sum_{n=-\infty}^{\infty} \delta\left(f - \frac{n}{t_s}\right)$$

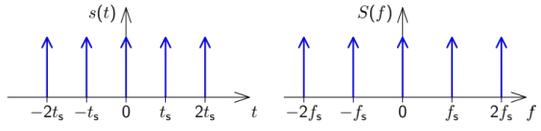


**Equation 8:** The Fourier Transform of the Dirac comb. This itself results in another Dirac comb, in the frequency domain. We originally can sample by a comb of Dirac impulses to obtain a sampled function $\hat{x}(t) = x(t) \cdot s(t)$ where $s(t)$ is defined above. This loss of information within a sampling process, converting a continuous function $x(t)$ into its discrete sequence $\{x_n\}$ may be defined by: $x_n = x(t_s \cdot n) = x(n/f_s)$. This discrete sequence may still be analysed by the FT on continuous functions.

**Figure 2**: This shows the Fourier Transform of a Dirac comb.

Given the following rectangular function, we have that its Fourier Transform is given by **Equation 9**, which is a (normalised) sinc function.

$$\mathrm{rect}(t) = \begin{cases} 1 & \text{if } |t| < \frac{1}{2} \\ \frac{1}{2} & \text{if } |t| = \frac{1}{2} \\ 0 & \text{otherwise} \end{cases}$$

$$\mathcal{F}\{\mathrm{rect}(t)\}(f) = \int_{-\frac{1}{2}}^{\frac{1}{2}} \mathrm{e}^{-2\pi \mathrm{j} f t}\, \mathrm{d}t = \frac{\sin \pi f}{\pi f} = \mathrm{sinc}(f)$$

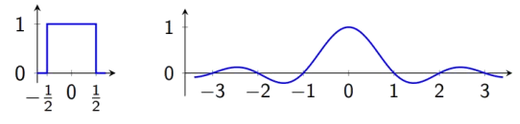


**Equation 9**: The Fourier Transform of the rectangular function, rect(t).

**Figure 3**: This shows the Fourier Transform of a rectangular function.

Therefore, putting this together in **Equation 10**, we have:

$$\mathscr{F}(I(p)) * \mathscr{F}(\{s(t)\}(f)) * \mathscr{F}(\mathrm{rect}(t))$$

**Equation 10:** The following expression denotes the result of the desired Fourier Transform of the range of $p_n$ further multiplied by a rectangular window.

From the Nyquist Theorem, which states we must sampled at least twice per waveform, which eliminates issues when convoluting with the Dirac comb, which can be ensured through the condition that the distance between samples is less than ½ λ.[13]

In spite of this, the convolution with the *sinc* function still results in leakage in spectral peaks, so a window is fitted manually through the multiplication of a window with a measured interferogram, by means of a window function, $W(p_n)$, which changes the spectral profile of the peaks observed. A Kaiser window with $\alpha = 3$ was selected, striking a compromise between the sharpness of peaks, and the reduction of spectral leakage.

### D. Mitigation of Other Effects

Other effects influence the quality of the interferogram[14], and the subsequent results from the analysed data, such as the Doppler width, pressure broadening, resonance broadening, self-reversal, as well as hyperfine structure, though most have negligible impact. The gas composition of the Hg lamp was found to consist of He, Ne, Ar and Kr, but at a low pressure (<100 Pa) with no effect.

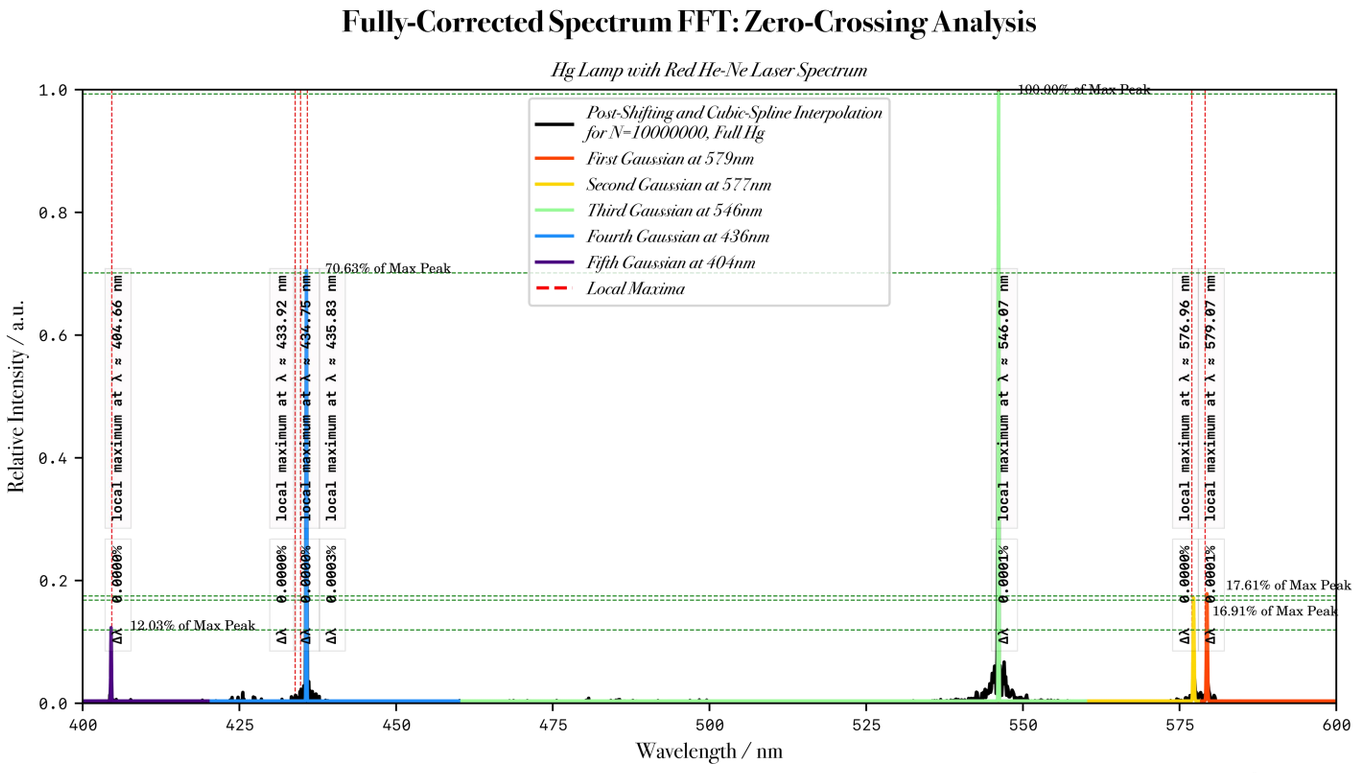


**Figure 3**: The resultant FFT spectrum from the interferogram taken for the red He-Ne laser with the mercury lamp. It can be shown that all the data observed is within 1Å of precision with the actual values, which demonstrates an extremely high degree of accuracy. We found that of the detected peaks, all five were in agreement with the Hg spectrum, as expected.

## V RESULTS

The following spectrum was obtained, as shown in **Figure 3** above, with each individual peak being included in the complementary insets accompanying it in **Figure 4**. A summary of the values of the theoretical peak as compared to the measured peak, as well as the FWHM and intensity, are found in **Table 1**.

**Figure 4** below, includes these aforementioned insets, which highlight a strong agreement between the theoretical values, and the measured values, all to a degree of precision of less than 2.5 parts in 10,000, or 0.00025%. This suggests that our interferometer was well calibrated and aligned, with sufficient adjustments.

| Theoretical Peak/Å | Measured Peak/Å | FWHM/Å | Relative Intensity/a.u. |
|---|---|---|---|
| **4046.563** Hg-I UV singlet | **4046.553** 0.00025% difference | **2.119** | **0.1231** |
| **4358.328** Hg-purple triplet III | **4358.521** 0.00004% difference | **2.224** | **0.7050** |
| **5460.735** Hg-I green singlet | **5461.355** 0.00014% difference | **1.177** | **1.0000** |
| **5769.598** Hg-I yellow doublet I | **5769.765** 0.00003% difference | **1.271** | **0.1724** |
| **5790.663** Hg-I yellow doublet II | **5791.081** 0.00007% difference | **1.239** | **0.1792** |

**Table 1:** The properties of the obtained spectral peaks, against NIST Hg spectral data.[15]

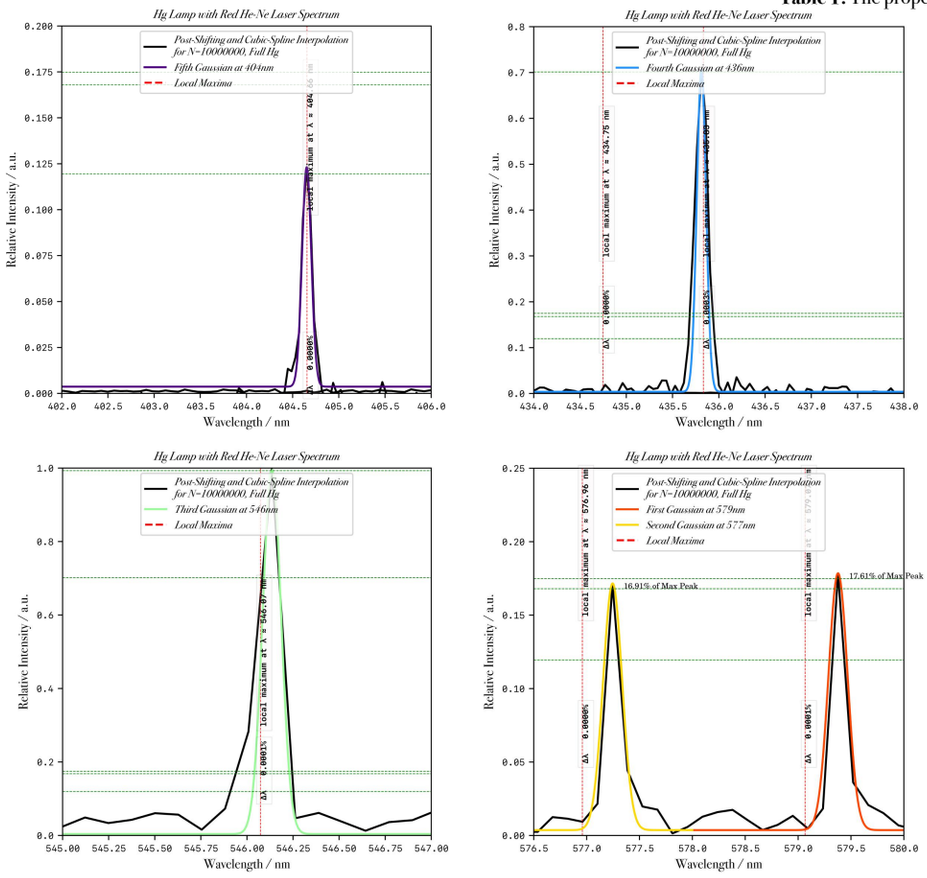


**Figure 4:** The complementary insets to **Figure 3**, of the five detected peaks, zoomed in.

The conspicious absence of the peaks: $\lambda = 4339.223$Å and $\lambda = 4347.494$Å, which compose the remaining two peaks of the violet triplet, suggests that they fell within the spectral leakage of a major peak at $\lambda = 4358.328$Å which meant they could not be resolved.

Additionally, we note that if we consider the value of the FWHM, all the theoretical peaks easily fit within this range. No additional spectral lines were obtained, which suggests that the lack of impurities in the Hg lamp that could've potentially introduced artifacts to the spectrum.

## VI CONCLUSION

In order to record an interferogram, a Fourier Transform Spectrometer was assembled, with the application of filters, use of calibration and a Kaiser window in order to correct the measured interferogram. Through the data processing of the interferograms, known peaks were found to be within a 2Å range, wich was a testament to the extreme precision of the experimental set-up.

Evidently, we could make several improvements in this experiment to further ameliorate the obtained data. The first would be to take an interferogram over a longer distance, though this would be difficult given we already took inteferograms over the entire range of the vernier calliper, so consequently the contraption would have to be elongated to allow for this possiblity. By increasing this, we would obtain data at a greater resolution, which would reduce the FWHM range. Peaks would also move closer to their actual theoretical values.[16]

We can further improve this contraption through a different stepper motor with smaller micro-step intervals, another means to increase the resolution. Further investigations may be conducted using other light sources, such as a white LED with coloured filters, as an extension, as was conducted but is omitted due to lack of space. This generalisation is possible to measure any spectrum given a particular light source, in order to study particular wavelengths. Further efforts to reduce the effects of Doppler width, pressure broadening, resonance broadening, self-reversal, as well as hyperfine structure would also be undertaken.

## VII Acknowledgements

First and foremost, I would like to thank my lab partner, Ollie Sharpe, without whom I would be unable to complete this practical as we both have a mutual dependency on each other, in particular with the practical aspects of this experiment, whilst I mostly conducted data analysis. His unbounded patience and due care was the only reason we were able to proceed at such breakneck pace. Next, I would like to thank the many people who stopped by our lab sessions after their own in order to offer their assistance such as: Arun Chonkaria, Endre Bokor, Jonte Catton, whom helped in many tricky areas such as the re-alignment of the He-Ne laser, as well as various mishaps we encountered related to gain and the Mercury lamps. I owe a huge debt of gratitude to the various lab technicians, in particular Ivan Hermida Estornell and Jay Hirani, whom came to my assistance at our darkest hours, and whom allowed us to stay in labs far longer than we were meant to. Last but not least, I have to thank the fantastic lab demonstrators, in particular Milan Ding, as well as Chris, Subu, James, Meizhen, and Bryony whom provided invaluable assistance when we were unable to proceed further.

## VIII References & Appendices

### Appendix I: Analysis and Curve-Fitting the Peaks

In order to determine the appropriate curve-fitting technique to use for the various spectral peaks in our Fourier Transformed data, we may apply either a Lorentzian, which makes for a better approximation due to the effects discussed in **Section IV.d**, or we may use a Gaussian, which is a slightly worse, but still reasonable approximation. For the Lorentzian, also known as the Cauchy distribution, we have that the probability density function (p.d.f.) is given by **Equation 11** as shown below.

$$f(x;x_0,\gamma) = \frac{1}{\pi\gamma\left[1+\left(\frac{x-x_0}{\gamma}\right)^2\right]} = \frac{1}{\pi}\left[\frac{\gamma}{(x-x_0)^2+\gamma^2}\right]$$

**Equation 11:** The probability density function of a Cauchy distribution.

Upon further examination, the improvements to the fitting by the Lorentzian were deemed too unimportant to warrant inclusion in the plots shown in **Figures 3** and **4**, since the main adjustments made by a Lorentizan are near the base of each peak, and area which does not concern us. Furthermore, the FWHM translates more nicely in the Gaussian than the Lorentzian distribution.

For the reasons listed above, only Gaussians were employed.

### Appendix II: The Notch and Band-Pass Filters

The expected effects of the notch and band-pass filters are shown in the following **Figures 5** and **6** below. The notch filter that was employed was the ThorLabs™ FB543.5-10 Laser Line Filter, with CWL = 543.5 ± 2nm, FWHM = 10 ± 2nm. It has a blocking range of 200 - 1150nm, and attempts to block out the He-Ne laser line. It has a $T_{min}$ of 70%.

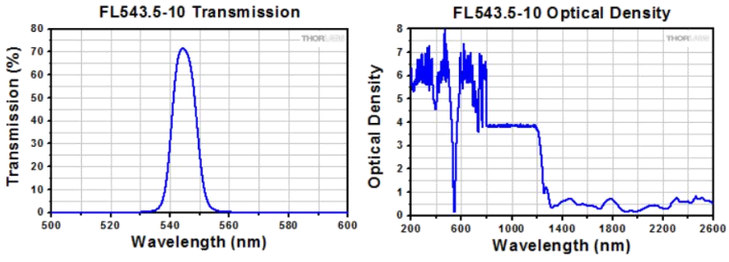


**Figure 5:** The transmission curve *(left)* and optical density *(right)* of the notch filter.

The band-pass filter employed was the ThorLabs™ FB580-10 filter, with 580 ± 2nm, FWHM = 10 ± 2nm. It has a blocking range of 200 - 3000nm, and doesn't attempt to block out any laser line in particular. It has a $T_{min}$ of 50%.

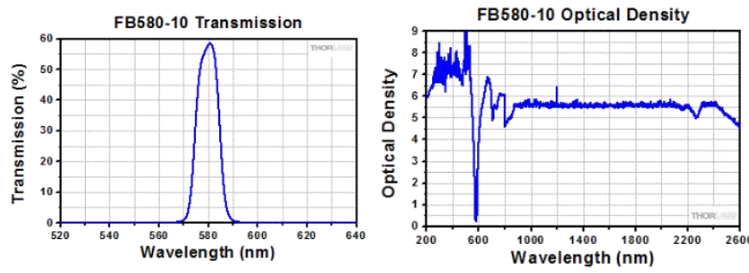


**Figure 6:** The transmission curve *(left)* and optical density *(right)* of the band-pass filter.

It was found that the notch filter, which we suspected to be another band pass filter, filtered out frequencies below 500nm, thus removing some crucial Hg data. Therefore, for some of the runs, we proceeded with the removal of the *"notch"* filter in order to gain this mercury data.

## References

[1] Colling, D. and Craplet, A. (no date) Blackboard Learn - Interferometry Lab Script, Interferometry Lab Script. Available at: https://bb.imperial.ac.uk/webapps/blackboard/execute/content/file?cmd=view&content_id=_2526822_1&course_id=_33949_1 (Accessed: February 8, 2023).

[2] Michelson Interferometric Set-Up (no date). LD Didactic. Available at: https://www.ld-didactic.de/documents/en-US/EXP/PHO/4747112EN.pdf (Accessed: February 8, 2023).

[3] Michelson Interferometers (no date) Course # 10: Module 4: Michelson interferometers. PhilPem. Available at: https://pe2bz.philpem.me.uk/Lights/-%20Laser/Info-999-LaserCourse/C10-M04-MichelsonInterferometers/Module10-4.htm (Accessed: February 8, 2023).

[4] Osram TOPLED®, SFH 2200 (no date) OSRAM TOPLED®, SFH 2200 | OSRAM Opto Semiconductors. Available at: https://www.osram.com/ecat/com/en/class_pim_web_catalog_103489/prd_pim_device_2219562/ (Accessed: February 8, 2023).

[5] Martin-HE543 - overview (no date) GitHub. Available at: https://github.com/martin-he543 (Accessed: February 8, 2023).

[6] Nema 17 Stepper Motor L=39mm gear ratio 100:1 high precision planetary gearbox (no date) STEPPERONLINE. Available at: https://www.omc-stepperonline.com/nema-17-stepper-motor-l-39mm-gear-ratio-100-1-high-precision-planetary-gearbox-17hs15-1684s-hg100 (Accessed: February 8, 2023).

[7] Thorlabs - HNL020LB HeNe laser, 632.8 nm, 2 MW, polarized, 100 - 240 VAC power supply included (no date) Thorlabs, Inc. - Your Source for Fiber Optics, Laser Diodes, Optical Instrumentation and Polarization Measurement & Control. Available at: https://www.thorlabs.com/thorproduct.cfm?partnumber=HNL020LB (Accessed: February 8, 2023).

[8] UVP® 90-0012-01 pen-ray® 11SC-1 Mercury UV lamp, 254nm shortwave, lighted length: 2.12-inches (no date) Capitol Scientific. Available at: https://www.capitolscientific.com/UVP-90-0012-01-Pen-Ray-11SC-1-Mercury-UV-Lamp-254nm-Shortwave-Lighted-Length-2-12-Inches (Accessed: February 8, 2023).

[9] Thorlabs - CCM1-BS013/m 30 mm cage cube-mounted non-polarizing beamsplitter, 400 - 700 nm, M4 TAP (no date) Thorlabs, Inc. - Your Source for Fiber Optics, Laser Diodes, Optical Instrumentation and Polarization Measurement & Control. Available at: https://www.thorlabs.com/thorproduct.cfm?partnumber=CCM1-BS013%2FM (Accessed: February 8, 2023).

[10] Eeeguide (2021) Second order low pass butterworth filter: Transfer function, EEEGUIDE. Available at: https://www.eeeguide.com/second-order-low-pass-butterworth-filter/ (Accessed: February 8, 2023).

[11] R. Bell, Introductory Fourier Transform Spectroscopy. Elsevier, 2012.

[12] Digital Signal Processing Exercises - University of Cambridge (no date). Cambridge University. Available at: https://www.cl.cam.ac.uk/teaching/1718/DSP/dsp-exercises.pdf (Accessed: February 8, 2023).

[13] James, J.F. (2015) A student's guide to fourier transforms: With applications in physics and Engineering. Cambridge: Cambridge University Press.

[14] Tolansky, S. (1986) An introduction to interferometry. Ann Arbor, MI: University Microfilms International.

[15] NIST Mercury Strong Lines (no date) Strong lines of mercury ( hg ). Available at: https://physics.nist.gov/PhysRefData/Handbook/Tables/mercurytable2.htm (Accessed: February 8, 2023).

[16] Helium-Neon lasers (no date) Sam's Laser FAQ - Helium-Neon Lasers. Available at: https://www.repairfaq.org/sam/laserhen.htm (Accessed: February 8, 2023).